Original Research Article

Theoretical Investigations of the Crystal Structures and Molecular Energetics of High Quality Silicon Carbide (*β*–SiC) Precursor Compound 1,4-bis(trimethylsilyl)benzene

ABSTRACT:

Over the last decades, the rapidly growing theoretical methods have revolutionized whole scientific paradigm, developed state-of-art analyses, and created substantial computational platforms through the huge support of outstanding mathematical algorithms. The self-consistent-charge density-functional based tight-binding (SCC−DFTB) scheme is one of them that offers versatile and efficient quantum mechanical calculations with some unique features compatible especially to the crystalline solid even at low computational resources. Its effective parametrizations and computational implementations under the *Gaussian* standardized interface as an "External program" via the users' script (*Gaussian− External* methodology; *GEM*) has added an additional value because of which various in-built high-level *Gaussian* computations are directly accessible. Herewith, the *Gaussian* offered geometry optimization algorithms & convergence criteria plus the *ModRedundant* type relaxed potential energy surface (PES) scanning techniques are assessed through the *GEM*, and characterized the crystal structures with concerned molecular energetics and PES of the experimentally synthesized 1,4-bis (trimethylsilyl) benzene (1,4–BTMSB) compound; a potential precursor for the high quality Silicon Carbide (*β*–SiC) coating particles, and an ideal "Internal Standard" for the quantitative spectroscopic analyses. The general results reveal that the 1,4– BTMSB molecules in its unit-cell and crystal lattice experience significant non-bonding interactions that induces them to attain the definite molecular geometry with recognizable ring, angle, torsional, & steric strains. The quantitative analyses of its PES depict that the phenylene ring has to overcome multiple yet unidentical energy barriers with the tallest $E_{a1} = 5.3\ kcal/mol$ in order to undergo internal 2π angular rotation around the 1,4–(**C–Si)** axes. And, exhibiting such type internal rotation of its phenylene ring is energetically highly probable as this compound is widely employed in coating high temperature reactors, and in quantizing analyte in high energy run spectroscopic facilities. The same quantification is referred here in order to underscore the significance of adopting perfectly closed topological molecular architectures while designing/synthesizing amphidynamic type crystalline free molecular gyrotops and their prototypes.

KEYWORDS: SCC−DFTB, "*Gaussian–External*", ***β*–SiC** Coating Particle, Spectroscopic "Internal Standard", and Monoclinic Crystalline Geometry.

1. INTRODUCTION

Being a precursor crystalline molecular compound for the complete syntheses of wide ranging chemical materials, and the monomeric prototype molecular compound for the construction of varieties of the silicon based polymers, the experimentally synthesized π-electronic system bridged bis-(trimethylsilyl) (hereafter, BTMS) based chemical compounds (**Fig. 1**) have gained substantial attentions in the recent decades [1–5]. Actually, such compounds are employed most frequently as a title compound due to possessing many recognizable physicochemical properties such as abnormal structural & chemical stability, rapid volatility property, better reactions optimizing & designing tendency, utmost possibility of functionalizing even *via* the transition metal–mediated chemical reactions, intramolecular charge transferring (ICT) features, $P2_1/n$ type stable monoclinic space group with two freely & independently aligned molecules per unit cell, relatively good participating ability in several industrially revolutionized coating methods (thermal spray, cold– spray, chemical vapor deposition (hereafter, CVD)), etc. [6–15]. For example, the 1,2-bis (trimethylsilyl)benzene compounds (**Fig. 1(A)**) are used in the synthesis of the (a) most potential benzyne precursors [1], (b) multifunctional & versatile 3D luminescent type boron–doped polymeric materials (emissive organic solid materials, electron-transporting materials, chemosensors, etc.) [2–5], (c) powerful Lewis-acid catalyst [6], (d) model chemical compound for the technologically advanced low molecular weight polymers [7, 8], etc. Similarly, the Bis-(trimethylsilyl)phenyl-bridged donor-acceptor molecules are used for (a) constructing the deep-blue emitting materials such as non-doped organic light-emitting diodes [7], (b) fluorescence quenching (restricting the molecular rotation in the excited states) [7], etc., the 1,4-bis (trimethylsilyl)tetrafluorobenzene (**Fig. 1(B)**) is used as a prototype for designing varieties of the title compounds required for the development of Si–based π–conjugated polymers (the most

emerging engineering materials in the fields of organic and hybrid solar cells) [9]. Comparatively, the experimentally synthesized monoclinic $P2_1/n$ type organosilicon crystalline compound 1,4-Bis (trimethylsilyl)benzene (appearance white crystalline powder; molecular formula $C_{12}H_{22}Si_2$; M_r = 222.4741; hereafter, 1,4-BTMSB) (number of molecules per unit cell Z = 2) [10,11] (**Fig. 1(C)**) is more recognizable due to its frequent uses in spectroscopic and industrial coatings such as (a) a secondary standard in quantitative NMR spectroscopy [12], (b) an internal standard in ^{1}HNMR spectroscopy [13], (c) a potential precursor for producing Beta type Silicon Carbide β–SiC; an impervious and hardest engineering materials (the degree of hardness is 9.25– 9.6, as close as 10 for the natural Diamond on Mohs scale) [14,15], (d) a better replacement for the traditionally used β– SiC precursor methyltrichlorosilane, (e) a fundamental source of the surface-hardened coating materials needful for the development of high temperature reactors (hereafter, HTR), etc. As per the critical literature analyses [14–24], the compound 1,4–BTMSB is found to be accepted widely as a far better precursor than the methyltrichlorosilane not only in terms of deriving better quality β–SiC particles but also their facile and efficient production steps, such as (a) compatible with the CVD operation techniques (even at high temperature (~1673 K)), (b) more stable & impervious, more oxidation & thermal shock resistance, and superior chemical inertness & mechanical strength, (c) more valuable & economic in designing tough, hard, and strong HTR basement (coating materials = mixture of UO_2 and β–SiC particles), (d) better in deposition even at mild conditions, and have less time dependency with the hardening processes, (e) more eco-friendly, and higher resistance to wearing, tearing, cracking, & corrosion, (f) more Cl_2 free, & less pyrophoric, (g) better in withstanding internal gas pressure, and in opposing chemical & high temperature effects, (h) good for minimizing HCl, Cl_2, UC, USi_2, and U_3Si_2 type fission products/byproducts released in the HTR technology, etc.

Besides all these effective and efficient uses, the crystalline 1,4-BTMSB compound has been extensively using in investigating primary roles of the molecular architectures and crystalline molecular geometries in order to design prototype molecular models that looks structurally analogous to the macroscopic rotor, gyroscope, and compass like devices; respectively known by the names molecular rotor, molecular gyroscope, and molecular compass in the nanometric world [25–27]. As these amphidynamic type crystalline molecular machines are designed/synthesized day-to-day with the greatest admiration of the latest computational/experimental techniques where the proper installation of the substituted/non-substituted dipolar/nonpolar rotary unit (such as phenylene) centrally through the Si–C type spinning axes joined both sides (1,4 positions) to the peripherally distributed three different explicit –$(Si–O)_x$– and Si–O–Si based siloxaalkane arms (stator) (**Fig. 2(A**) and **Fig. 2**(**B**)) (closed topology) is a key in maintaining many potential parameters of the crystals (packing coefficient C_K, free space around the rotary segment (free–volume), rotational energy barrier E_a) that act as the most fundamental prerequisites for functionalizing crystalline free–rotators successfully [28–33], the proper evaluations, quantifications, and the most appropriate justifications for all these structure–correlated parameters are only possible if they are examined with 1,4-BTMSB's open topological molecular architecture precisely *via* some potential computational/theoretical and/or experimental means. To materialize the same, the crystalline 1,4-BTMSB compound is very often treated as a reference molecular compound in both experimental and theoretical research works [26–28] while exploring how effectively the peripheral static frameworks of the molecular gyroscopes/compasses/rotors can block the intermolecular force of interactions (interactions between the periodic molecular arrays, interactions between the rotators of the intervening molecules, interactions between the rotators

and stators, etc.) so that their central rotary segments experience negligible hindrance, and significantly low E_a which in fact leads the entire molecular architectural pathways towards the development of functional crystalline free molecular machines. Present author and his collaborators have already reported those rigorous works elsewhere [26–29, 31–33] where the amphidynamic crystalline siloxaalkane molecular gyroscopes /compasses with the perfectly closed structural topologies are dealt impressively with respect to the qualitative results computed for the open topological molecular structure of 1,4-BTMSB compound.

Despite being 1,4-BTMSB crystalline compound a center of interest for the various state– of–art applications, the in-depth structural characterizations of its monoclinic crystal structure and the two independent molecular alignments inside its unit-cell plus the detailed quantum mechanical computations of the rotational potential energy surface (hereafter, PES) for its 1,4–Si–linked phenylene segments with respect to the peripheral methyl groups & the exact estimation of E_a with enough clarifications given on the basis of structural topologies (open topology; 1,4-BTMSB compound, **Fig.1 (C)**) vs closed topology; molecular gyroscope/compass, **Fig. 2(A)** and **Fig. 2(B)**) by incorporating the most significant and predominant type van der Waals (hereafter, vdW) type non-bonding interactions exist in between the trimethylsilyl groups $-Si(CH_3)_3$ & each explicit methyl group/s of the neighboring molecules are yet to be reported. Beside this, to the knowledge of the present author, the structural stabilities of its crystalline molecular geometry at different intermittent positions of the PES such as local minima, global minima, saddle points, etc. are far from the researchers' consideration. Since in the NMR and GS– MS spectroscopies where the magnetic field of $1–20T$, and the electron energy of $70eV = 1614\, kcal/mol$ are applied respectively for the custom analysis of the chemical compounds, the 1,4-BTMSB crystal as an "internal standard" is observed to produce the

chemical shifts at 0.0 ppm (similar to the tetramethylsilane TMS peak position because of having four magnetically equivalent aromatic protons and eighteen equivalent methyl protons), and its *m/z* value with 100% abundance at 207 (molecular ion peak, $M_r(222) - M_r(CH3)$ (15)) by retaining its molecular entity [34]. It means the monoclinic crystal of the 1,4-BTMSB can resist relatively as equal energy as this without undergoing any crystalline structural breakages and spectroscopic malfunctions, and most probably with undergoing induced type internal rotation of its phenylene unit across the 1,4-(Si–C) axes. In this sense, the in-depth examinations of the extra stable structural entities of its unit-cell at each theoretically evaluated points on the rotational PES are needful. In fact, the proper addressing of these issues can only be assessed if the intense effects of the vdW force of interactions experienced by the entire unit-cell, and phenylene segments of each molecule (the phenylene unit feel strong force of interactions with the trimethylsilyl groups of the same molecule (intra–molecular) as well as of the nearby molecules (inter–molecular) arranged periodically in the definite crystalline phase) are taken into account. As this type force is very much responsible to determine the electronic/structural stabilities/instabilities, structural abnormalities, bonding/angular (dihedral angle) irregularities/dislocations of the molecules in respect to 1,4-(Si–C) axes (**Fig. 1(C)**), & their periodic arrays, and is primarily originated from the structural congestion created steric hindrance, the only possible means for taking into consideration of them solely are the effective implementation of the most suitable computational methodologies that have adopted advanced yet promising quantum mechanical formulations. To the experience of the present author, one of such potent computational means is "Extended Density-Functional based Tight-Binding Scheme (hereafter, DFTB+)" [35–40]. It is widely recognizable quantum mechanical software package that integrates many more spectacular

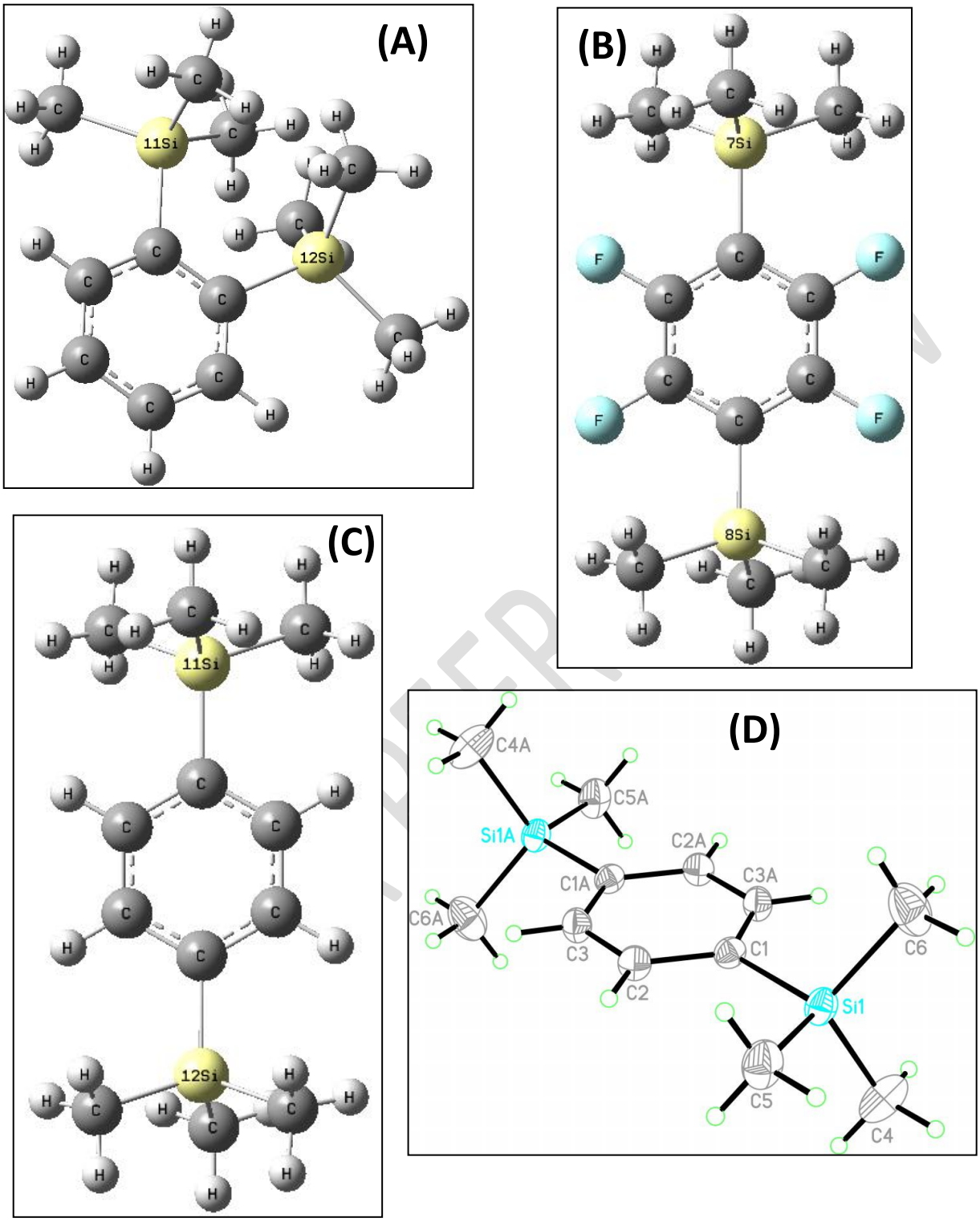

Fig.1. A GaussView sketched experimentally synthesized π-electronic system bridged bis-(trimethylsilyl) based open topological molecular entities; (**A**) 1,2-bis(trimethylsilyl)benzene, (**B**) 1,4-bis-(trimethylsilyl)tetrafluorobenzene, (**C**) 1,4-Bis-(trimethylsilyl)benzene, (**D**) an XRD structure of (**C**) with the atom numberings reproduced from ref [10].

mathematical / computational schemes designed especially to overcome the several intrinsic

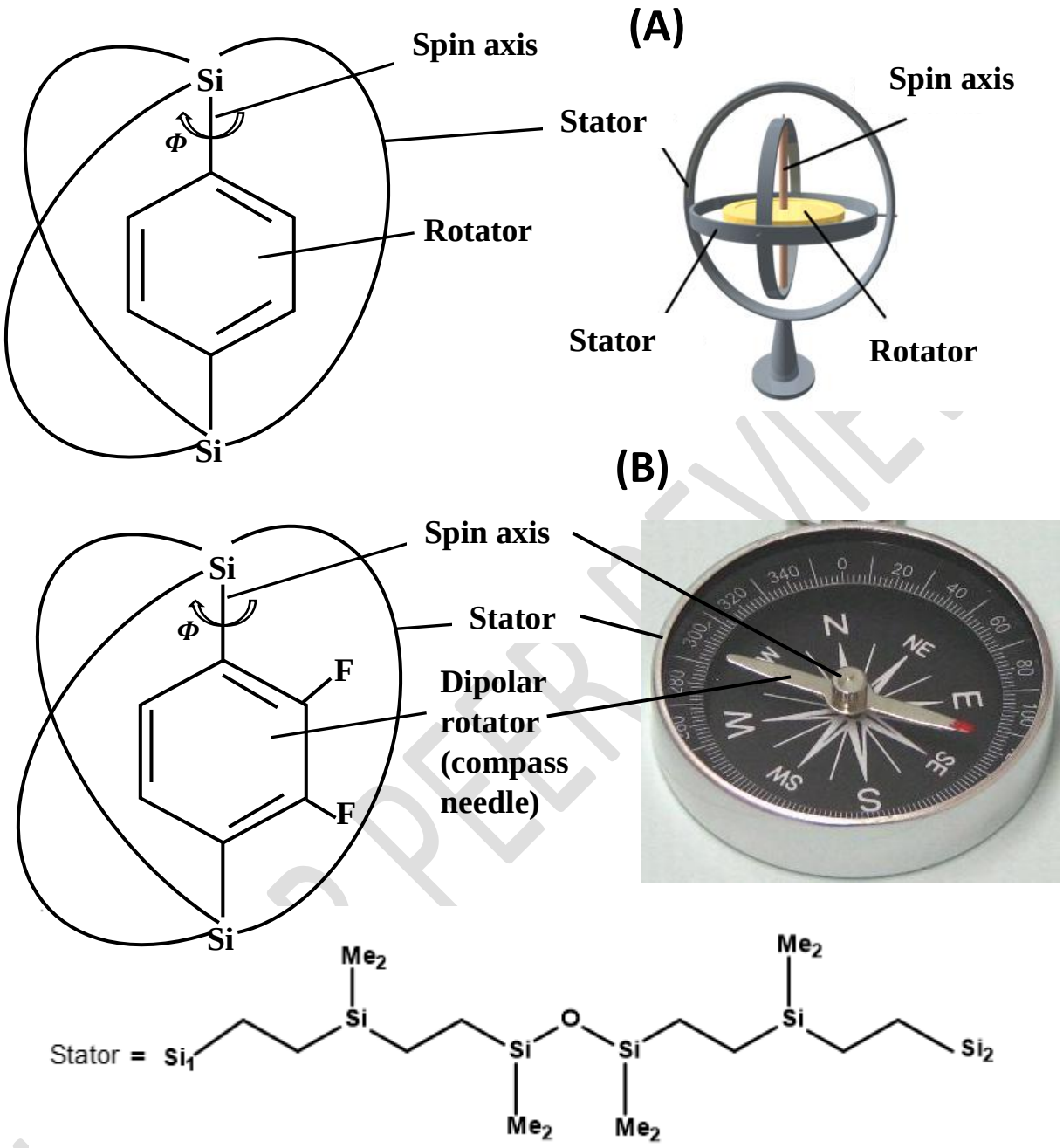

Fig.2. A schematic diagram of the 1,4-bis-(**Si**)–linked π-electronic system bridged molecular gyroscope and compass with the closed topological molecular entities; (**A**) a crystalline molecular gyroscope with a non-polar phenylene rotator, (**B**) a crystalline molecular compass with a dipolar difluorophenylene rotator (compass needle). The respective experimentally synthesized molecular analogues for them are firstly reported by Setaka *et al.* herewith [26, 27] with using three long siloxaalkane spokes (represented by three arcs) explicitly. In terms of their structural topology and functions, they resemble quite close to the macroscopic gyroscope and compass respectively as depicted pictorially.

limitations of the solid state chemistry. Among them, the "Dispersion Energy Corrections"

algorithm of it is relatively more demandable not only due to efficient executing ability of the Slater−Kirkwood model but also implementing Slater−Koster files (SK−files) routinely with giving an additional focus to the solid state crystalline systems. The DFTB+ operates all these rigorous formulations via the (a) Non-Self-Consistent-Charge DFTB (NCC− DFTB); a zeroth-order expansion of the Kohn-Sham total energy in DFT with respect to charge density fluctuations, and (b) Self-Consistent-Charge DFTB (SCC−DFTB); a second-order expansion, schemes [38–41]. While the former is known with its traditional features applicable mainly to treat the nonpolar and homonuclear molecular systems mathematically [41], the latter is preferably chosen here due to its quantum mechanical treatment to the charge distribution in a molecule (point charges) obtained through the iterative self-consistent manner, relatively more promising features to cope with the heteroatomic molecular systems where the charge balance between the atoms is crucial [38,39], and superb performance in computing crystal geometries & molecular energetics of the amphidynamic type molecular crystals [28–33]. This article is organized as: in section 2, the detailed Materials and Methods are outlined; in section 3, the Results and the relevant Discussions are presented, and in section 4, the concise Conclusions are expressed.

2. MATERIALS AND METHODS

As per the X–ray crystallography reported elsewhere [10, 11], the monoclinic, $P2_1/n$ crystal of 1,4-BTMSB (number of molecules per unit cell, $Z = 2$) has a unit cell dimensions $a = 6.5410$ Å, $b = 10.5452$ Å, and $c = 10.3952$ Å. The mercury crystallographic software [42(a)] was used to extract the concerned unit-cell parameters; $a, b, c, \alpha, \beta, \gamma$ from the concerned crystallographic information file with *.cif* extension, and also the X–ray derived unit-cell Cartesian coordinates explicitly. Thus derived unit-cell Cartesian coordinates were used

collectively as its trial structure for the entire computations. Since the whole DFTB+ itself, and its most potential SCC–DFTB type scheme lacks some additional computational features that are as similar as *Gaussian's* "*ModRedundant*"; the computational mean responsible to perform relaxed PES calculations; the *Gaussian–External* methodology offering a substantial ability of calling SCC–DFTB scheme via the user provided scripts as an "*External Program*" was employed computationally, and accessed the *Gaussian's* features efficiently. The detailed computational procedure that routes this methodology under the *Gaussian's* standardized interface is summarized in **Scheme 1**. As per the requirements of this methodology, the unit-cell

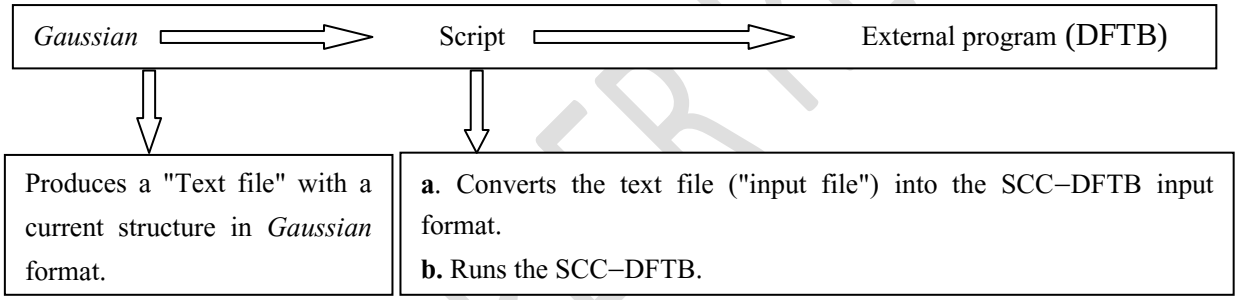

Scheme. 1. Working procedure of the *Gaussian-External* methodology

Cartesian atomic coordinates of the 1,4-BTMSB were used explicitly in the *Gaussian* text-file format, and the entire geometry was fully optimized with the *Gaussian optimizer* under the SCC–DFTB offered PBC + "*Dispersion Energy correction*" platforms. While scanning the rotational PES of the phenylene unit in respect to its predefined dihedral angle ϕ (the standard definition of ϕ is given in **Fig. 3**), the *Gaussian* action code "***S***" followed by the controllers "*nsteps stepsize*" were explicitly mentioned in the text–file, and computed the concerned electronic energy at each redundant geometry constrained with the specific ϕ scaled up by the *stepsize* $+2^\circ$ (clockwise scanning) and -2° (anticlockwise scanning) from its original (experimentally observed) value $\phi = 36.6^\circ = 0.203\pi$ (moduloπ). It means both the *Gaussian's*

"optimizer and *Modredundant"* plus the DFTB's "*Dispersion Energy Correction*" features were implemented at the same time through the *Gaussian − External* methodology, and the ground state 3D equilibrium structure of the unit-cell plus the corresponding structural entities at each local/global minimum & saddle point of the PES were computed. The *Jmol* graphics [42(b)], and its "*Measurement*" tools were used to render the structures in 3D space, and to determine all the concerned structural parameters.

The "Input file" with the required "*Keywords*" for the "*External Program*" was created programmatically by referring the DFTB+ manual available elsewhere [43]. The Hamiltonian operator and its associates recommended for the crystalline states were configured through the "*Hamiltonian = DFTB*" followed by "*Periodic = Yes*, & *Lattice-Opt = Yes*" tags. The Brillouin zones integration was executed under "*KPointsAndWeights*", and each explicit set of the lattice vectors extracted from the *.cif* file was appended. The "*NoSymm*" terminology was selectively used to block the symmetry breakage of the molecules/unit-cell during the entire computational iterations. The Cartesian coordinates format of the unit-cell was put into effect by "*Geometry= GenFormat*" driver, and each recurring geometry was appended serially in a separate text file via "*AppendGeometries = Yes*" function. The SCC type iterations were ensured through the "*SCC=YES*" procedure, and the required "*SCCTolerance*" ($1e{-}5$) and "*MAXSCC Iterations*" (200) were set as tight as *Gaussian*. Moreover, the vdW type nonbonding interactions were taken into account by "*Dispersion = SlaterKirkwood*" scheme, and all the required dispersion constants such as polarizabilities α (Å^3), Slater–Kirkwood effective numbers N_{eff}, cutoff interaction range r_c, and the effective charge (*Chrg.*) for each and every atoms with a unique coordination were supplied under the "*HybridDependentPol*" tag. The concerned parameter sets for the **H**, **C**, and **Si** atoms of 1,4–BTMSB were taken from those sets that were established

earlier for the closed topological molecular gyroscopes/compasses, and many other heteroatomic crystalline systems [28,43]. For accessing the Slater–Koster files (*.skf* extension) of every pairwise permutation atomic types, the *mio–1–1* and *pbc–0–2a* sets were used computationally.

3. RESULTS AND DISCUSSIONS

3.1 Unit Cell Geometry of Crystalline 1,4–Bis(trimethylsilyl)benzene Compound

The *Gaussian–External* methodology operated "*External Program*" SCC–DFTB with "*Dispersion Energy Correction*" features derived low energy electronic structure of the isolated 1,4-BTMSB molecule, and its entire unit-cell (no. of molecules per unit cell $Z = 2$) rendered through the *Jmol* graphics are displayed in **Fig. 3**, and **Fig. 4** respectively. For the comparative purpose, the X–ray diffraction characterized unit-cell structure rendered through the same visualization tool is also shown in **Fig. 5**. All the atoms labeled in **Fig. 3** are as per the definition of the structural parameters bond lengths, bond angles, and dihedral angles listed in **Table 1**, and these descriptors were set based on the quantitative explanations and structural characterizations to be carried out in this study. For example, the chemical bonds C2–C3, C1–C2, C3–C4, etc. are selected to quantify the ring strains of the C1–Si7, C4–Si8 linked phenylene unit; the bond angles such as C6–C1–C2, C5–C4–C3, C4–C3–C2, etc., and H6–C6–C1, H2–C2–C1, C6–C1–Si7, C5–C4–Si8, etc. are selected to deduce its interior and exterior angle strains respectively, the dihedral angles such as C6–C1–Si7–C73, C2–C1–Si7–C73, C5–C4–Si8–C81, C3–C4–Si8–C81, etc. are selected to explain its torsional strain; the bond angles such as C73–Si7–C72, C72–Si7–C71, C71–Si7–C73, C83–Si8–C82, C82–Si8–C81, C81–Si8–C83, etc. are selected to theorize the steric strains experienced by the three non-bonding tri-methylsilyl groups (two set) attached to Si7 and Si8 atoms peripherally, the bond angles H711–C71–H713, H811–C81–H812, etc. are selected to examine the tetrahedral orientation of the hydrogen atoms

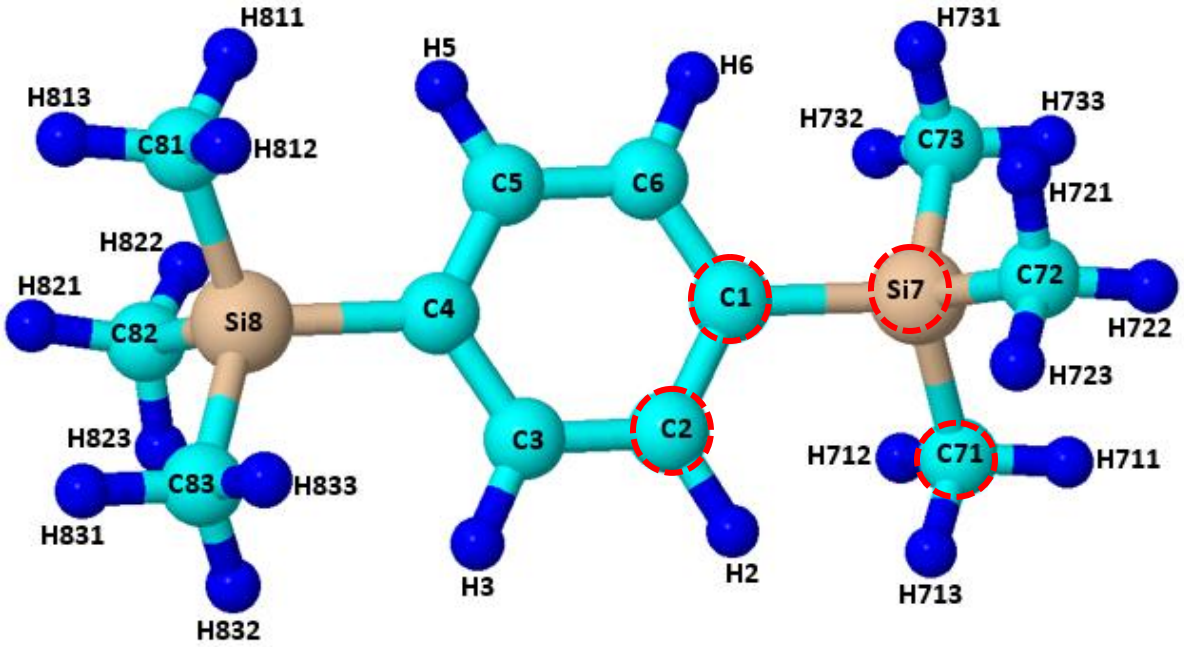

Fig.3. A "SCC–DFTB + PBC + Dispersion Energy Corrections" optimized structure of an isolated molecule present in the unit-cell of 1,4-BTMSB crystalline compound. All the atoms are numbered as per the measurement definitions of bond lengths (Å), bond angles (°), and dihedral angles (°) summarized in Table 1. The optimized geometry of the entire unit-cell of this molecule is shown in **Fig.4.** The definition of the dihedral angle is given by the atoms C2–C1–Si7–C71 encircled in red colored shapes. The theoretically predicted dihedral angle between the planes formed by these atoms is highlighted by red color in **Table 1**.

of each methyl (CH_3) group explicitly; and the distances measured in between any two non-bonding atoms and groups such as C2– – C5, C2– – C6, C72– – C73, Si7– – Si8, Si7– – C3, etc. are selected to justify all those strains in terms of phenylene ring alignment, and tri-methylsilyl substituents' 3D configuration.

As shown in **Table 1**, all the phenylene C−C bond lengths are theoretically computed as 0.140 nm in average. This bond distance is longer than the standard carbon-carbon double bond ($l_{C=C} = 0.134nm$) but shorter than the standard carbon-carbon single bond ($l_{C-C} = 0.147nm$); ensuring us the presence of partial double bond characters in phenylene ring with significant effects of the delocalized π-electrons. Similarly, the theoretically predicted interior and exterior

bond angles are 117.7 °(involving *ipso* C atom) & 121.2 °(involving *meta* & *para* **C** atoms), and

Table 1. Experimental *Expt.* vs. Theoretical *Th.* (*SCC–DFTB + PBC + Dispersion Energy Correction*) structural parameters for the 1,4-BTMSB molecule measured in its unit cell

1,4-BTMSB molecule	**Magnitude of the Bond Lengths (*nm*) and Bond Angles (°)**			
	Expt. (nm)		***Th.(nm)***	
Structural parameters (Bonds and Angles)	**Ref. 10**	**Ref. 11(a)**	**Ref. 11(b)**	**This study**
C1–C2 (C1–C6)	0.13994 (0.140)	0.1393	0.141	0.140 (0.141)
C2–C3 (C5–C6)	0.13946	0.1376	0.139	0.140
C4–C5(C4–C3)	0.13946	0.1395	0.141	0.141
Si7–C1 (Si8–C4)	0.18817	0.1891	0.185	0.187
Si7–C71 (Si8–C81)	0.18622	0.1831	0.188	0.187 (0.186)
Si7–C72 (Si8–C82)	0.18622	0.1885	0.188	0.187 (0.187)
Si7–C73 (Si8–C83)	0.18622	0.1895	0.188	0.186 (0.187)
C1– – C3 (C5)	–	–	0.245	0.244
C1– – C4	–	–	0.289	0.285
C1– – C71 (C72, C73)	–	–	0.305	0.304 (0.303, 0.305)
C1– – C81 (C82, C83)	–	–	0.566	0.563 (0.558, 0.564)
C2– – C5	–	–	0.276	0.278
C2– – C6	–	–	0.239	0.241
C71– – C72	–	–	0.378	0.307
C72– – C73	–	–	–	0.304
C71– – C73	–	–	–	0.304
Si7– – Si8	–	–	0.660	0.659
Si7– – C2	–	–	0.286	0.285
Si7– – C3	–	–	0.417	0.410
Si7– – C4	–	–	0.475	0.472
Si7– – C81(C82, C83)	–	–	0.744	0.743 (0.743, 0.738)
C1– – H2 (H6)	–	–	0.215	0.217 (0.218)
C1– – H3 (H5)	–	–	0.342	0.343 (0.343)
C1– – H711	–	–	0.400	0.399

C1– – H712	–	–	0.324	0.319
C1– – H713	–	–	–	0.331
C1– – H811	–	–	0.672	0.666
C1– – H812	–	–	0.557	0.541
C1– – H813	–	–	–	0.574
C2– – H3	–	–	0.213	0.216
C2– – H5	–	–	0.384	0.388
C2– – H6	–	–	0.337	0.341
C71– – H721	–	–	0.328	0.325
C71– – H722	–	–	0.327	0.322
C71– – H723	–	–	0.404	0.401
Si7– – H2	–	–	0.298	0.298
Si7– – H3	–	–	0.500	0.501
Si7– – H711	–	–	0.248	0.248
Si7– – H712	–	–	–	0.247
Si7– – H713	–	–	–	0.247
Si7– – H811	–	–	0.852	0.848
Si7– – H812	–	–	0.728	0.712
Si7– – H813	–	–	–	0.748
C2– – C71	–	–	0.329	0.337
C2– – C72	–	–	0.402	0.378
C2– – C73	–	–	0.423	0.433
C2– – C81	–	–	0.548	0.542
C2– – C82	–	–	0.497	0.508
C2– – C83	–	–	0.479	0.470
C3– – C71	–	–	0.467	0.472
C3– – C72	–	–	0.521	0.501
C3– – C73	–	–	0.537	0.546
C3– – C81	–	–	0.437	0.429
C3– – C82	–	–	0.371	0.388
C3– – C83	–	–	0.347	0.334
C71– – C81	–	–	0.857	0.858
C71– – C82	–	–	0.822	0.803
C71– – C83	–	–	0.791	0.796
C6–C1–C2	–	115.8	115.7	117.7
C5–C4–C3	–	115.8	115.7	117.7
C4–C5–C6	–	122.8	–	121.2

C4–C3–C2	–	121.4	–	121.1
C6–C1–Si7	–	–	–	121.6
C5–C4–Si8	–	–	–	121.0
C2–C1–Si7	–	–	–	120.7
C3–C4–Si8	–	–	–	121.3
C71–Si7–C1	–	107.8	–	109.1
C73–Si7–C72	–	109.9	–	109.1
C72–Si7–C71	–	108.5	–	110.7
C71–Si7–C73	–	–	–	109.5
C81–Si8–C82	–	109.4	–	110.5
C82–Si8–C83	–	109.4	–	109.2
C81–Si8–C83	–	109.4	–	109.5
C83–Si8–C4	–	111.0	–	109.7
C81–Si8–C4	–	110.2	–	109.4
H6–C6–C1	–	–	–	119.9
H2–C2–C1	–	–	–	119.7
H3–C3–C4	–	–	–	119.9
H5–C5–C4	–	–	–	119.9
H711–C71–H713	–	–	–	109.4
H721–C72–H723	–	–	–	109.5
H811–C81–H812	–	–	–	109.4
H821–C82–H822	–	–	–	109.4
C6–C1–Si7–C73	–	–	–	–24.7
C2–C1–Si7–C73	–	–		156.6
C2–C1–Si7–C71	**–**	**–**	**–**	**36.6**
C5–C4–Si8–C81	–	–	–	–35.5
C3–C4–Si8–C81	–	–	–	145.6
C6–C5–C4–C3	–	–	–	0.0
C2–C3–C4–C5	–	–	–	0.1
C5–C6–C1–C2	–	–	–	–0.6
C3–C2–C1–C6	–	–	–	0.7

119.7 ° in average respectively. These values are deviated from the respective bond angles measured in the regular planar shaped benzene molecule (bond angle= 120.0°). It further guaranties the existence of notable angular strain in the ring as predicted by the gas phase

electron diffraction technique [11(b)]. Therewith, the respective interior angles are reported as 115.7° in average. The exactly similar type bond angles determined from the oscillation & Weissenberg photographs and the visual estimation of the intensities are reported as 115.8°, and 121.5° in average elsewhere [11(a)] (Table 1). Interestingly, all these theoretically and experimentally predicted angular values are found to be quite consistent to each other. In addition to this, the geometric relationship of the phenylene ring with the peripherally distributed trimethylsilyl substituents is described herewith via the critical analyses of the dihedral angles computed in this studies. Actually, the small change in dihedral angles between the planes formed by them always leads to the substantial change in structural conformation, and in this case, their closed investigations may reveal the exact alignment of the phenylene ring along the C1–Si7, and C4–Si8 axial bonds. The dihedral angles concerned with this such as C2–C1–Si7–C73, C2–C1–Si7–C71, C3–C4–Si8–C83, C5–C4–Si8–C81, etc. are listed in **Table 1** which not only confirms the slightly twisted shape of the phenyene ring across the two planes that intersect at the C–Si axes but also supports the experimental evidences speculated ring strains. These sets of the dihedral angles further guaranties that there is an existence of the relatively stronger torsional strength between each methylsilyl group and phenylene ring. Unlike this, the steric strain experienced by the three non-bonding methyl groups attached to each Si7 and Si8 atom is revealed as negligible as the bond angles between them such as C71–Si7–C1; C73–Si7–C72; C72–Si7–C71; C71–Si7–C73; C81–Si8–C82; C82–Si8–C83, etc. are predicted theoretically as 109.5° in average; a standard tetrahedral angle consistent to that of the experimentally derived value (*Expt.* = 109.4° in average) [11(b)]. The 109.5° angular gap between each methyl group in respect to the central Si7 and Si8 atoms plus the perfectly tetrahedral 3D configuration of its H atoms (H731–C73–H733; H711–C71–H712;

H832−C83−H831; H**81**1−C81−H812 etc. type bond angles listed in **Table 1**) signify the

existence of negligible non-bonding interactions or repulsive steric interactions between the

atoms and groups. As a whole, all these dissimilar strains observed in 1,4-BTMSB molecule

such as ring strain, angle strain, torsional strain, steric strain, etc. are justified collectively herewith by the distances measured in between some of the preselected non-bonding atoms (– – is used to denote non-bonding case) and groups as listed in **Table 1** such as: (a) C2– – C5, C2– –

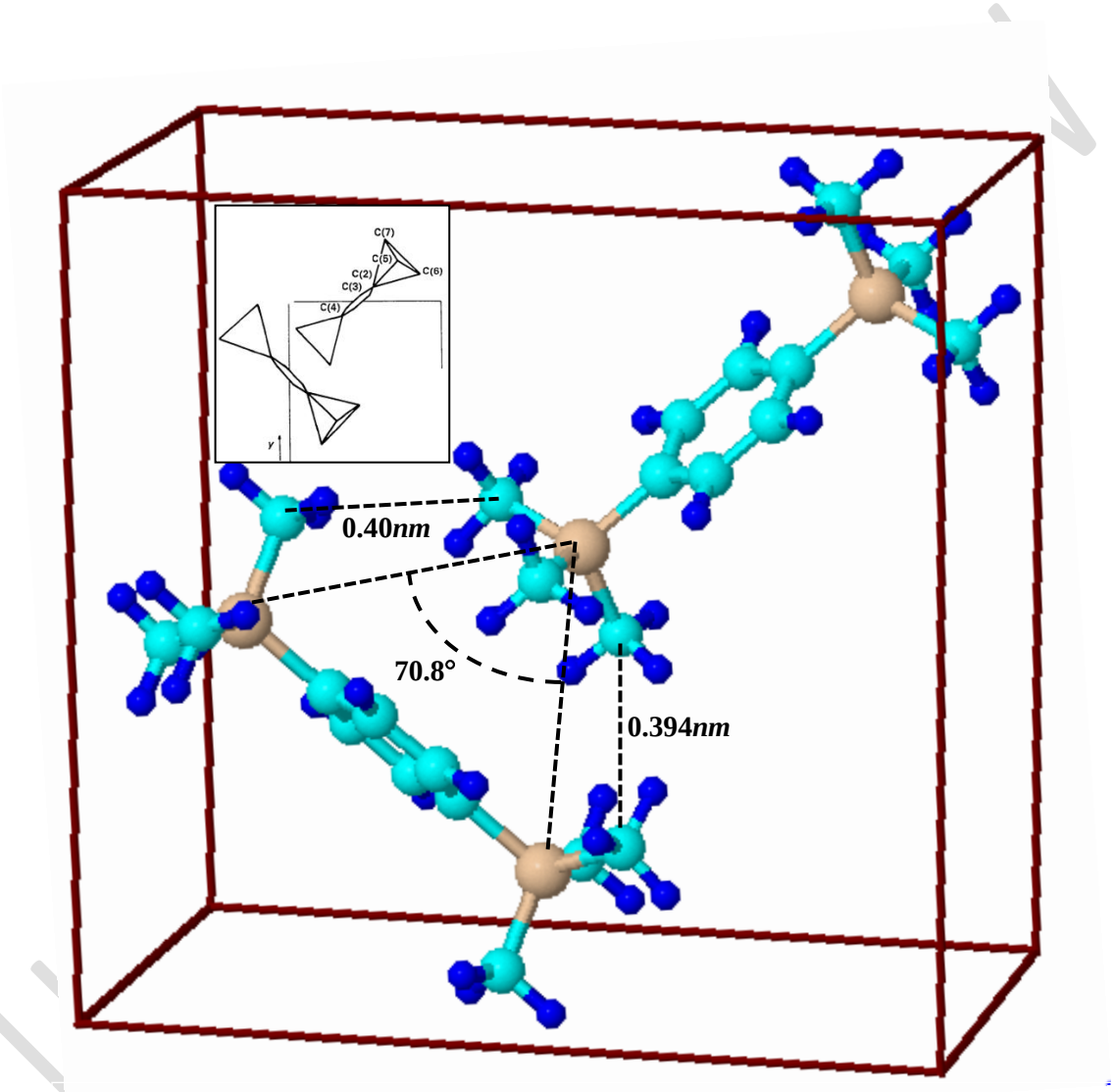

Fig.4. A "SCC–DFTB + PBC + *Dispersion Energy Corrections*" optimized structure of the unit-cell of 1,4-BTMSB crystalline compound with bounding box. The two molecules present in its unit-cell are aligned based on the XRD predicted projections (ref. 11(b)) onto the (100) lattice plane (as shown in the inset). The cyan, blue, and gray spheroids represent C, H, and Si atoms

C6, etc. distances that are theoretically predicted in the range of $0.388nm$ and $0.341nm$

respectively; the quite reasonable values to that of the experimentally determined datasets ($0.384\ nm$, and $0.337\ nm$) reported by Rozsondai *et al.* elsewhere [11(b)]; quantify the trimethylsilyl groups caused internal ring strain as the same set of the distances measured in the regular planar benzene molecule with no steric groups attached to its ipso carbon atoms at all are $0.279\ nm$ and $0.242\ nm$ respectively; (b) C1– – C3 (C5), C1– – C4, etc. distances *Th.* $0.244\ nm$ (*Exp*. $0.245\ nm$) and *Th.* $0.285\ nm$ (*Exp.* $0.289\ nm$) respectively depict the slightly elongated or outward stretched phenylene ring towards the ipso 1,4–C corners as the similar type distances in a regular nonstrained benzene with no any substituents are measured as $0.241nm$ and $0.279\ nm$ respectively; (c) C1– – C71 (C72, C73), C1– – C81 (C82, C83), etc. distances *Th.* $0.304\ nm$ (average, *Exp.* $0.305\ nm$), and *Th.* $0.563\ nm$ (average, *Exp.* $0.566\ nm$) respectively describe the direction and intensities of the phenylene ring and its trimethylsilyl-groups' deformation. In conclusion, all such type outward expansion, elongation, and the entire structural deformation of the 1,4–BTMSB molecule in its unit-cell are mainly caused by the electronegativity of the trimethylsilyl groups as expected. Since the trimethylsilyl groups are principally recognized as the appreciable electronic resonance interaction groups that show strong abilities to exert direct influence on the phenylene ring attached to them on either side of the **Si** atoms, and are known for their exceptional electron-releasing tendencies (the electronegativity difference between **Si** and **C** is $+0.7$ unit on the Pauling scale) [44], the direct strains put by them on the phenylene ring resulted all those structural irregularities and abnormalities. More precisely reiterating, all those electronic and structural strains experienced by the phenylene ring, and its peripheral trimethylsilyl groups are as a result of the intense van Der Waals type intra– and inter– molecular interactions: the phenylene ring feel strong force of interactions with its sideways distributed trimethylsilyl groups (intra–molecular), and themselves

are interacted with the neighboring molecules (inter–molecular) arranged periodically in the

monoclinic crystalline patterns. And, the principal cause of originating such type nonbonding

interactions is none other than the structural congestion created steric hindrance. Therefore, the closeness of the two molecules in the unit-cell approximate the strength of the van Der Waals type forces between them, and is estimated herewith by the distances measured in between some of the pre-selected non-bonding atoms (**Fig.4** and **Fig. 5**): the nearest non-bonding C– – C, and

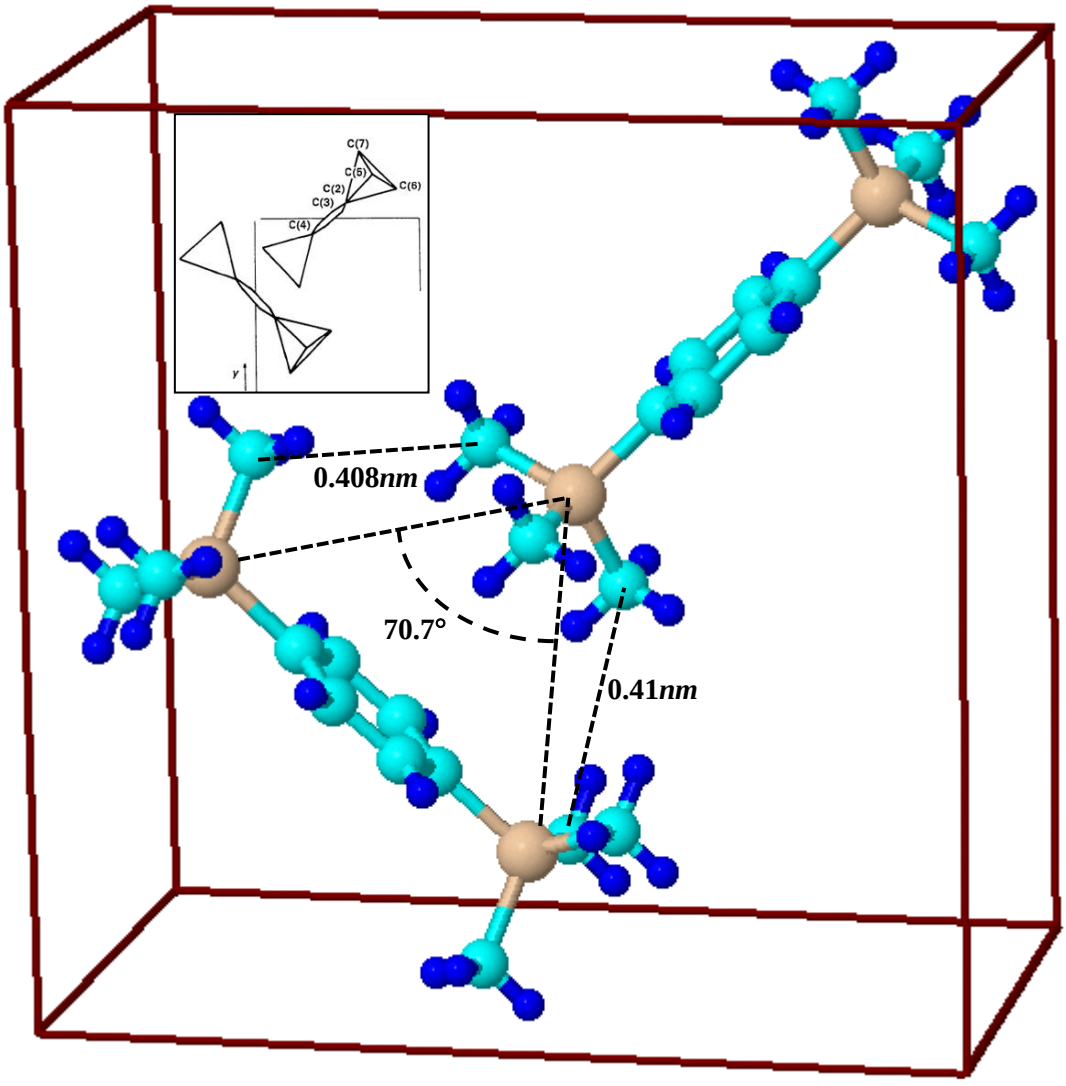

Fig.5. A *Jmol* rendered XRD characterized unit-cell structure of the 1,4-BTMSB crystalline compound with bounding box. The two molecules present in its unit-cell are aligned based on the XRD predicted projections (ref. 11(b)) onto the (100) lattice plane (as shown in the inset). The cyan, blue, and gray spheroids represent C, H, and Si atoms respectively.

H– – H distances between the two molecules of the unit-cell are theoretically predicted as $0.361\ nm$ (*Exp.* $0.401\ nm$ [11(a)]), and $0.281\ nm$ respectively. In fact, the closest distance that the two atoms of the nearby molecules can approach to each other must always exceed sum of their van der Waals atomic radii, the nearest molecular gap predicted in this study validates it well: as an example, sum of the van der Waals atomic radii between the two **C** atoms = $(0.17\ +\ 0.17)\ =\ 0.340\ nm$ which is smaller than the distance computed for the C– – C ($0.361\ nm$)) of the two nearby molecules. Based on this evaluation, one may conclude that the two molecules aligned in the theoretically derived unit-cell maintain a just-required amount of the intermolecular gap even while close-packing of their unit-cells repeatedly in the crystal lattice. In terms of the distances & angular departures in respect to nearby methyl groups and molecular elongation plane (each Si atom of each molecule in the unit-cell is inclined by 70.8° (*Expt.* 70.7°) angle in respect to the nearby molecular elongation plane, and each methyl group of each molecule is departed by the distance in average of $0.41\ nm$ (*Expt.* $0.40\ nm$) with the nearby methyl group of another molecule (**Fig. 4** and **Fig. 5**,)), the two molecules are also found to maintain a just enough gap required to undergo tight molecular packings with notable packing coefficient C_k; a mandatory characteristic features of the crystalline solid.

Besides all these explicit structural characterizations of the 1,4–BTMSB molecules and their unit-cells, present study also focuses on how closely the theoretically derived unit-cell geometry resembles with the experimentally reported crystal structure. As displayed in **Fig. 4** and **Fig. 5**, the X–ray produced and "SCC–DFTB + *Dispersion Energy Corrections*" optimized three dimensional electronic structures seem alike to each other. Even the 3D orientations and the related structural conformations of each and every methylsilyl groups attached to Si7 and Si8 atoms, and the overall structural alignment of the phenylene ring are reproduced by the present

theoretical methodology semiquantitatively. As a whole, the entire molecular alignments in the unit-cell and the peripheral orientations of every methylsilyl groups plus the relative positions of the phenylene rings in respect to C4–Si8 and C1–Si7 axes are exactly similar to the XRD predicted projections onto the (100) lattice plane as shown in the insets of **Fig.4** and **Fig.5**. Energetically, the theoretically computed electronic energy of the global minimum electronic structure is $E = -337.171761 E_h$ (relative Energy$E_r = 0.0\ kcal/mol$); a $\sim$5.3 $kcal/mol$, and $\sim$1.8 $kcal/mol$ times less energy structure than the structures computed at first saddle point and first local minimum as noted on the PES plotted in **Fig. 6**. The more detailed energetic point of view is expressed in the subsection 3.2.

3.2 Potential Energy Surfaces

The computational incorporation of the monoclinic crystalline molecular assembly of the 1,4–BTMSB compound with two molecules per unit-cell (number of atoms in each molecule $= 36$) while the concerned computations are in the fly is a challenging task in terms of utilizing computational resources, and executing complex mathematical formulations. In the view of *ab initio* perspectives offered by the *Gaussian* package, such calculations are regarded as computationally expensive, and time consuming plus suddenly interrupted during iterative procedures types. The computational incorporation of the "*Dispersion Energy Corrections*" features under PBC further demands more computational efficiencies and resources with additional mathematical algorithms. Towards resolving these obstacles and frequent failures, and more importantly smooth proceeding of the entire computational procedures genuinely without worsening the computational accuracies and mathematical precisions, present study employed SCC–DFTB scheme under *Gaussian–External* methodology so that both the DFTB+ and *Gaussian* offered features get simultaneous access. The *Gaussian's* "*ModRedundant*" feature

assessed through the *Gaussian–External* methodology was employed to compute the relaxed PES. Under this feature, the dihedral angle ϕ defined in **Fig.3** (C71–Si7–C1–C2 is highlighted in **Table 1**) was stepped up by +2° (clockwise scanning) and –2° (anticlockwise scanning) from the original value $\phi = 36.6^\circ = 0.203\pi$ (moduloπ) measured in the optimized unit-cell geometry displayed in **Fig.4**, and the PES was scanned in between 0π to 2π with the computations of corresponding Eigen values E and unit-cell structures at each redundant ϕ. The graphical mathematical function that shows a relationship between the E, and the specific molecular geometry (i.e., atomic position) redundant at each predefined ϕ; literally called potential energy surface, is shown in **Fig.6** where the global, and local minima plus the saddle points are explicitly marked. The unit-cell geometries computed to these theoretically evaluated points on the PES, and their 1π degenerate structures are shown in **Fig.7**.

As shown in **Fig. 6**, the SCC–DFTB computed PESs with and without "*Dispersion Energy Correction*" features are almost reproducible to each other along with the locations of the global and local minima, saddle points plus their degenerate positions on them. They are respectively observed at $\phi = 0.2\pi(\#1)$, $\phi = 0.7\pi(\#2)$, and $\phi = 0.9\pi(\#3)$ radians whose corresponding degeneracies are appeared at $\phi = 1.3\pi(\#1')$, $\phi = 1.7\pi(\#2')$, and $\phi = 1.9\pi(\#3')$ radians respectively. As expected, the PES derived by addressing "*Dispersion Energy Corrections*" under PBC (red colored curve in **Fig. 6**) displays more recognizable yet reproducible degenerate minima, and estimates relatively taller energy barrier $E_{a1} = 5.3\ kcal/mol$ in between the first global $(\#1)$ and local minima $(\#2)$ as it was slightly underestimated to the value $E_{a1} = 4.3\ kcal/mol$ while excluding "*Dispersion Energy Corrections*" features. This observation justifies the need of incorporating all the intra– and inter– molecular type non-bonding interactions existing in the 1,4– BTMSB molecular crystal

computationally throughout the computational procedures of deriving crystal structures and molecular energetics. Therefore, the SCC–DFTB approach equipped with the "*Dispersion Energy Corrections*" inscribed Slater–Kirkwood polarization algorithm is regarded as a superb theoretical scheme. Additionally, the energy barrier exists in between the first local minimum $(\#3)$ and the second global minimum $(\#1')$ is $E_{a2} = 3.0\, kcal/mol$ which is also extremely underestimated to $E_{a2} = 1.78\, kcal/mol$ in the absence of "*Dispersion Energy Corrections*" features. Towards deducing the effects of structural topologies of the molecular compounds, the energy barrier $E_{a1} = 5.3\, kcal/mol$ estimated for the crystalline 1,4–BTMSB compound with completely open type structural topology is highly useful. This magnitude of E_{a1} is found to be incomparable to that computed for the **Si** and **–(Si–O)$_x$–** based molecular gyroscopes (flipping barrier $E_a = 1.2\, kcal/mol$), and molecular compasses ($E_a = 4.9\, kcal/mol$) simply due to having perfectly closed structural topologies (**Fig. 2**). This structural role on reducing E_a foresees the most essential credentials required to design functional crystalline free molecular architectures, and influences the synthetic chemists to set most effective strategical synthetic laboratorial pathways. Based on the same analyses, present author, and his theoretical/ experimental collaborators referred 1,4–BTMSB crystalline compound time to time while investigating the working mechanisms of the molecular gyroscopes and compasses plus their most possible applications (dichroism, birefringence, etc.) in the nanometric world [25–33]. Therewith, the extreme importance of the peripherally distributed flexible type **Si** & **–(Si–O)$_x$–** made siloxaalkane spokes that encapsulates the rotary phenylene unit centrally plus their effective practical adoptions in designing state-of-art molecular architectures and prototype gyrotops that can exhibit macroscopic gyroscope/compass like functions facilely were quantified by the various sophisticated experimental and theoretical approaches. Besides this, the steric

strains (intra–/ inter– molecular) experienced by the central phenylene rotator of such designed molecular gyroscopes/compasses were theorized based on the open structural topology of the 1,4–BTMSB compound possessing a similar type phenylene unit but strained sterically with the six

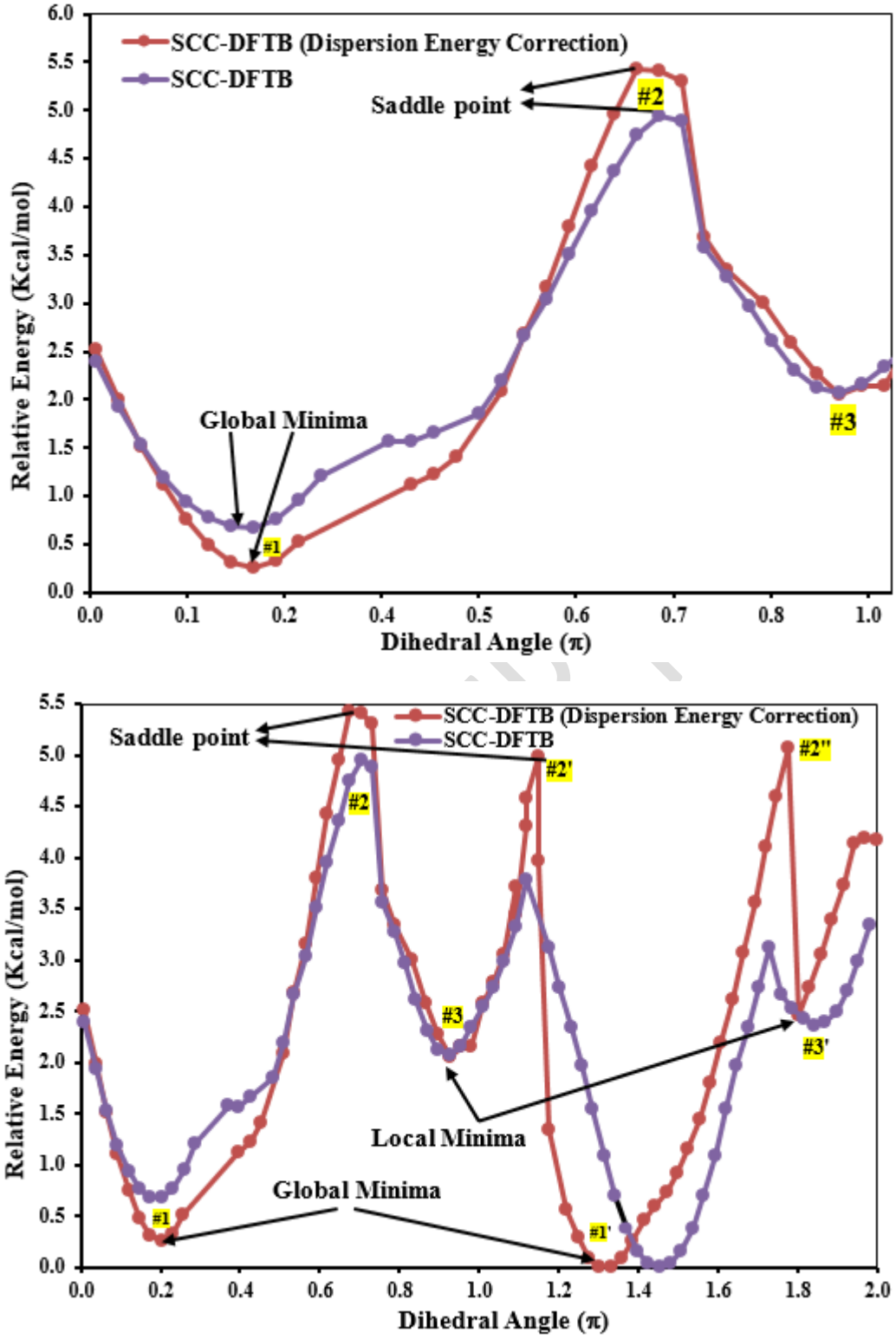

Fig.6. The *Gaussian–External* operated SCC–DFTB derived potential energy surfaces (PES) with and without "*Dispersion Energy Corrections*" features under periodic boundary condition (PBC). The concerned dihedral angle ϕ that was fixed throughout the PES scanning calculations is defined in **Fig. 3.** The corresponding unit cell geometries at each minimum and saddle point are shown in **Fig. 7.**

trimethylsilyl groups configured peripherally on its either sides. Additionally, the "Free Volume" (free space) unit available around the rotary segment of the molecular gyroscopes/compasses was precisely evaluated, and appropriately justified in reference to the open topological molecular architecture of the same crystalline molecular compound, and nowadays it is regarded as an essential parameter while upgrading & inventing various other gyroscopic molecular prototypes. Towards all these quantitative perspectives, the present theoretical investigations associated with determining molecular crystal structures, PESs, activation energy barriers E_a, global/local minima

& saddle points plus their explicit geometrical entities, and their in-depth correlations of the extensively using 1,4–BTMSB compound put significant values.

Moreover, the structural and geometrical stability of the unit-cell of the 1,4-BTMSB compound, and its entire monoclinic crystal structures matters a lot while justifying the extra stability, indestructibility, mechanically more durability, and the surface-hardened characteristic features of its β type silicon carbide β–SiC coating particles because of which this crystalline compound is actually accepted as a far better precursor than the traditionally used methyltrichlorosilane in terms of advancing high temperature reactor (HTR) technologies [14–24]. In addition to this, the extensive uses of this crystalline molecular compound as a secondary standard in quantitative NMR spectroscopy [12], and as an "internal standard" in quantitative analysis of small organic molecules in ^{1}HNMR spectroscopy demand thorough examination of its structural stabilities & unit-cell moieties at different equilibrium and non-equilibrium stages of the rotational pathway of the phenylene ring *viz.* rotational PES (**Fig. 6**). In these sense, the structural visualizations and theoretical characterizations of the stable unit-cell geometries at different global/local minima, saddle points, and their respective degenerate

positions are meaningful. Therefore, present study explicitly reports herewith all the unit-cell structures that belong to each

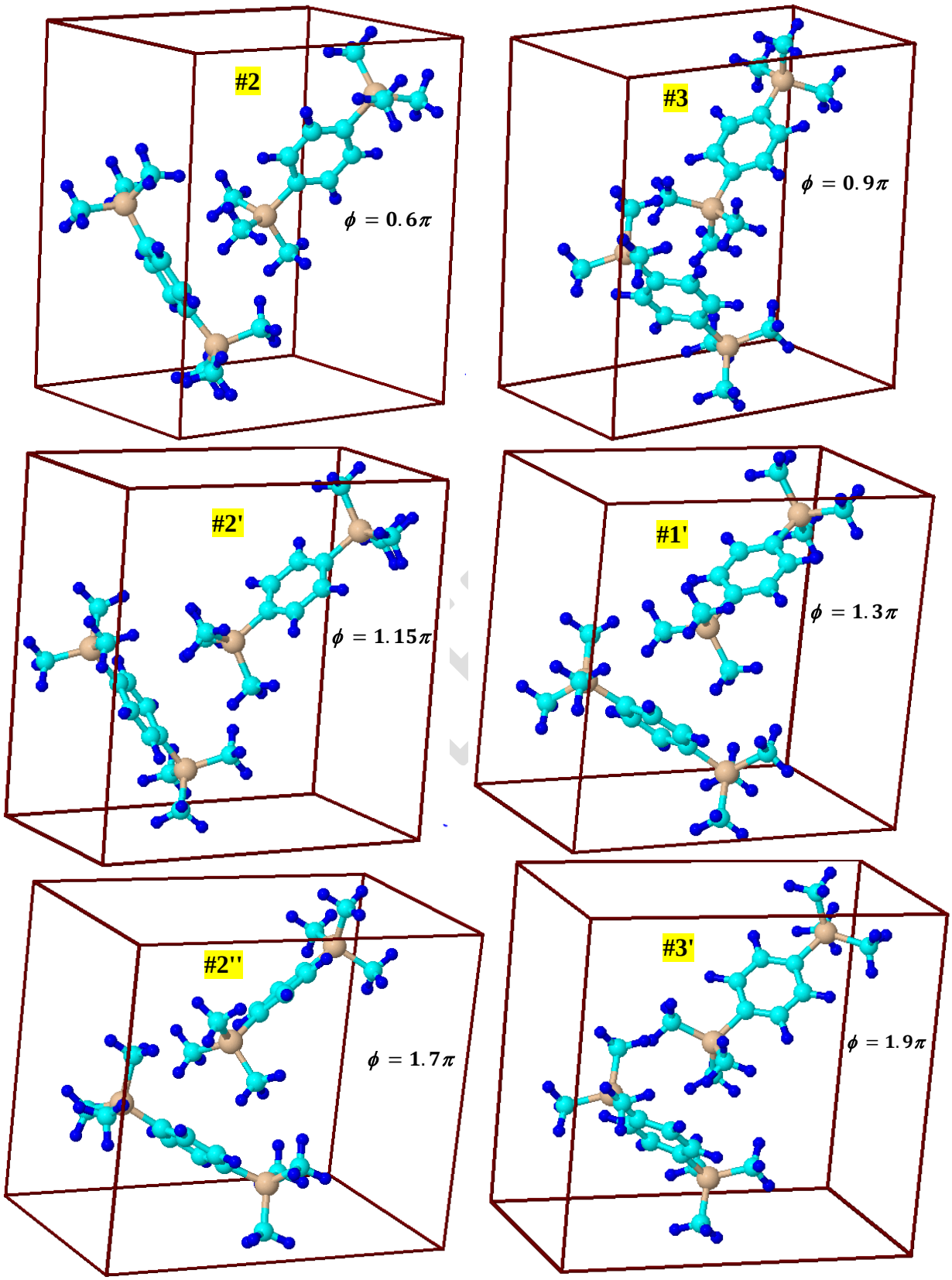

Fig.7. The *Gaussian–External* operated SCC–DFTB produced unit cell structures of the global/local minimum, saddle points, and their degenerate positions. The specific symbols used to mark them on the potential energy surface are mentioned in the inset where the concerned dihedral angle ϕ is explicitly given. While rendering these images, the major attention was given in the molecular entity and molecular alignments rather than the angular position of the phenylene

and every theoretically evaluated points of the PES. As shown in **Fig.7**, they are structurally differed to each other by the specific dihedral angle ϕ. All the structurally unobstructed unit-cell entities and the geometrically unconfined molecular configurations of each of them ensure their stability at different intermittent rotary forms of the phenylene ring even while undergoing smooth induced type internal rotation at ambient/high temperature (T) ranges (sources: HTR technology, NMR and ^{1}HNMR spectroscopies, etc., and this specific temperature may enable the phenylene ring to overcome concerned energy barrier $E_{a1} = 5.3\ kcal/mol$ facilely. In fact, the $K_B T = 0.60\ kcal/mol$ when $T = 300\ K$, whereK_B and T are Boltzmann constant and absolute temperature, respectively). To the knowledge of this author, the most probable happening of the internal rotation of the phenylene ring of the 1,4-BTMSB compound is logical as it is not only used as a potential precursor of the high quality coating particles required for the HTR technologies but also as an internal standard in various spectroscopic facilities run with high electronic energy and magnetic fields.

4. CONCLUSION

This theoretical study was mainly focused to investigate the crystal structures and molecular energetics of the high quality silicon carbide (β–SiC) precursor, and the spectroscopic "Internal Standard" compound 1,4-bis(trimethylsilyl)benzene (1,4–BTMSB) theoretically. Based on the complexity of the monoclinic crystalline patterns of this compound, and its relatively bigger unit-cell structures with two molecules ($Z = 2$, no. of atoms per molecule = 36) plus the limited availability of the computational resources and the computational/theoretical features demanded by this specific study, present author employed *Gaussian–External* methodology that genuinely offers an integrative ways of functionalizing low– yet decent– level quantum mechanical schemes as an "*External–Program*" under the standardized interface of the *Gaussian*,

and of utilizing thus produced Eigen values (optionally a dipole moment or forces) at each specific molecular geometry via the users' provided "*External–Script*". For the sake of addressing predominant effects of the hetero-atomic charge distributions & charge density fluctuations, and the entire van Der Waals type intra– and inter– molecular force of interactions in the molecular structure of 1,4–BTMSB, the SCC–DFTB parametrizations was run computationally as an "*External–Program*" as it enables the chemists to treat the former effects by SCC type iterative calculations, and the latter by "*Dispersion Energy Corrections*" inscribed Slater–Kirkwood polarization algorithm. And, for computing relaxed potential energy surface (PES), the *Gaussian's "ModRedundant"* technique was assessed via the *Gaussian–External* methodology.

The closed structural analyses of the *Gaussian–External* operated "SCC–DFTB + *Dispersion Energy Corrections*" optimized unit-cell structures under the periodic boundary condition (PBC) revealed that the molecules of the 1,4-BTMSB in its crystal lattice and unit-cell experience significant non-bonding interactions that induce them to attain recognizable ring strain, angle strain, torsional strain, and steric strain. The theoretically derived structural descriptors such as bond lengths between the bonding and non-bonding atoms/groups, bond angles, dihedral angles, etc. that collectively discloses all those structural strains were found to be quite reproducible to the electron/X–ray diffraction, and oscillation & Weissenberg photographs predicted datasets. Contrastingly, the theoretically estimated angular gap between each methyl group of its two sets of trimethylsilyl groups uncovered their three dimensional tetrahedral configurations with negligible repulsive steric interactions. Similarly, the theoretically predicted nearest non-bonding **C– – C**, and **H– – H** distances between the two molecules present in its unit-cell; $0.361nm$ (*Exp.* $0.401nm$) and $0.281nm$ respectively;

signified the degree of their closeness which in turn was useful to approximate the strength of their binding force (van Der Waals type force). As a whole, while comparing its phenylene ring position, each methysilyl groups peripheral orientations, and phenylene ring relative alignment in respect to 1,4–(**C−Si)** axes, the theoretically produced unit-cell geometry was found to be exactly similar to that of the XRD predicted structures projected onto the (100) lattice plane. Additionally, the in-depth quantitative analyses of its PES derived in respect to each redundant dihedral angle ϕ depicted that the phenylene ring has to cross multiple yet unidentical energy barriers in order to undergo internal 2π angular rotation around the 1,4– (**C−Si)** axes. The tallest energy barrier estimated was $E_{a1} = 5.3\ kcal/mol$; a relatively low in magnitude that can be overcome by its phenylene ring while employing the crystalline 1,4-BTMSB compound at moderate/higher temperature ranges ($K_B T = 0.60\ kcal/mol$ when $T = 300\ K$) such as in the production of high quality β–**SiC** coating particles, in the high temperature reactor (HTR) chemical vapor deposition (CVD) techniques ($T \cong 2000\ K$), in the quantitative spectroscopic analyses (source: electronic energy ($70ev$, and magnetic fields $20T$), etc. The detailed structural examinations and the related molecular energetics computed at different theoretically evaluated points on the rotational PES that supported the most probable occurrence of the internal rotation of the phenylene at relatively high temperature ranges unveiled that the molecular entities in the unit-cells remain intact and structurally composite even while undergoing this specific type internal movement. Beside this, the nature of the PES and its barriers explained the degree of ineffectiveness of 1,4–BTMSB's molecular architectures in terms of the requirements of the molecular gyroscopes/compasses/rotors, and their functions plus underscored the significance of adopting perfectly closed topological molecular architectures while designing/ synthesizing latter type amphidynamic crystals.

Series of the publications that were concentrated into the 1,4–BTMSB compound so far are found to be reported its precise yet modified synthetic routes, title compounds and the required structural redeterminations/modifications, conveniently accessible yet efficient reactions pathways producing high percentage yields, direct employment in HTR coatings via CVD techniques, inestimable potentiality in producing economically viable yet mechanically durable and impervious type coating materials, etc. To the knowledge of this author, none of the research papers hypothesized and theorized the possibility of undergoing internal rotation of its structurally strained & stressed phenylene ring and, the associated structural/energetic stabilities & molecular integrities in the unit-cell while utilizing its crystal as an "Internal Standard" in the high-energy/ temperature run experimental facilities and a precursor in deriving better quality ***β*–SiC** particles. Towards this rigorous part, present theoretical investigations and examinations added a praiseworthy value. In materializing and strengthening the interpretations given in this report, other genuine experimental/theoretical studies are recommended.

REFERENCES

1. Lorbach A, Reus C, Bolte M, Lerner HW, Wagner M. Improved Synthesis of 1,2-Bis (trimethylsilyl)benzenes using Rieke-Magnesium or the Entrainment Method. Advanced Synthesis and Catalysis. 2010; 352:3443–3449.
2. Saito S, Matsuo K, Yamaguchi S. Polycyclic π-Electron System with Boron at Its Center. Journal of American Chemical Society. 2012; 134:9130−9133.
3. Dou C, Saito S, Yamaguchi S. A Pentacoordinate Boron-Containing π- Electron System with Cl−B−Cl Three-Center Four-Electron Bonds. Journal of American Chemical Society. 2013; 135(25):9346–9349.

4. Yamaguchi S, Akiyama S, Tamao K. Colorimetric Fluoride Ion Sensing by Boron-Containing π-Electron Systems. Journal of American Chemical Society. 2001; 123:11372–11375.
5. Yamaguchi S, Wakamiya A. Boron as a key component for new π–electron materials. Pure and Applied Chemistry. 2006; 78(7):1413–1424.
6. Dobos S, Szabo A, Zelei B. Vibrational Spectra and IR Dichroism of p-bis (trimethylsilyl)benzene. Spectrochimica Acta, Part A: Molecular Spectroscopy. 1976; 32 (7):1393–1399.
7. Shen Z, Zhu X, Tang W, Zheng Y, Zhou Z, Feng XJ, Zhao Z, Lu H. Bis(trimethylsilyl) phenyl-bridged D-A molecules: Synthesis, spectroscopic properties and for achieving deep-blue emitting materials. Dyes and Pigments. 2020; 174:108063(1–8).
8. Mori MN, Yoshida IVP. Synthesis and characterization of some poly-p-silphenylenes, Polymer Bulletin. 1992; 29:35-42.
9. (a) Finze M, Reissb GJ, Frohn HJ. 2, 3, 5, 6-Tetrafluoro-1,4-bis(trimethylsilyl)Benzene, Acta Crystallographica Section E. 2012; 68(Pt4):o1082.

   (b) Mdluli SB, Ramoroka ME, Yussuf ST, Modibane KW, John-Denk VS, Iwuoha EI. π–Conjugated Polymers and Their Application in Organic and Hybrid Organic-Silicon Solar Cells. Polymers. 2022; 14(4): 716(1–37).
10. Haberecht M, Lernera HW, Bolte M. p-Bis(trimethylsilyl)benzene: rerefinement against new intensity data. Acta Crystallographica Section E. 2002; E58; o436–o437.
11. (a) Menczel G, Kiss J. p-Bis(trimethylsilyl)benzene. Acta Crystallographica. 1975; B31, 1787–1789.

(b) Rozsondai B, Zelei B, Hargittai I. The molecular structure of p-bis (trimethylsilyl)-benzene from gas phase electron diffraction. Journal of molecular structure. 1982; 95; 187–196.

12. Rundlof T, McEwen I, Johansson M, Arvidsson T. Use and Qualification of primary and secondary standards employed in quantitative ^{1}H NMR spectroscopy of pharmaceuticals. Journal of Pharmaceutical and Biomedical Analysis. 2014; 93:111–117.
13. Pinciroli V, Biancardi R, Colombo N, Colombo M, Rizzo V. Characterization of small combinatorial chemistry libraries by 1H NMR. Quantitation with a convenient and novel internal standard. Journal of Combinatorial Chemistry. 2001; 3(5):434–440.
14. Selvakumar J, Sathiyamoorthy D, Nagaraja KS. Role of vapor pressure of 1,4-bis (trimethylsilyl)benzene in developing silicon carbide thin film using a plasma-assisted liquid injection chemical vapor deposition process. Surface and Coatings Technology. 2011; 205:3493–3498.
15. Selvakumar J, Sathiyamoorthy D, Nagaraja KS. Solid-state kinetics and gas-phase prediction of 1,4-bis(trimethylsilyl)benzene. Journal of Thermal Analysis and Calorimetry. 2012;109(1):113–122.
16. Mellor BG, Guilemany JM, Nin J. Thermal Spraying Methods for Protection Against Wear. 2006; Ch. 8. pp. 249–301.
17. Filatova EA, Hausmann D, Elliott SD. Understanding the Mechanism of SiC Plasma-Enhanced Chemical Vapor Deposition (PECVD) and Developing Routes toward SiC Atomic Layer Deposition (ALD) with Density Functional Theory. ACS Applied Materials and Interfaces. 2018; 10(17):15216–15225.

18. Chin J, Gantzel PK, Hudson RG. The structure of chemical vapor deposited silicon carbide. Thin Solid Films. 1977; 40:57–72.
19. Allendorf MD, Kee RJ. A Model of Silicon Carbide Chemical Vapor Deposition. Journal of The Electrochemical Society. 1991; 138(3):841–852.
20. Pillari R, Batra N, Manocha LM, Machinewala N. Deposition of silicon carbide interface coating on carbon fiber by PECVD for advanced composites. Surfaces and Interfaces. 2017; 7:113–115.
21. Yao R, Feng Z, Chen L, Zhang Y, Zhang B. Preparation and characterization of freestanding SiC (Ti, B) films derived from polycarbosilane with TiN and B as additives. Journal of the European Ceramic Society. 2012; 32(10):2565–2571.
22. Drieux P, Chollon G, Jacques S, Allemand A, Cavagnat D, Buffeteau T. Experimental study of the chemical vapor deposition from CH_3SiHCl_2/H_2: Application to the synthesis of monolithic SiC tubes. Surface and Coatings Technology. 2013; 230(15):137–144.
23. Iliescu C, Poenar DP. PECVD Amorphous Silicon Carbide (α-SiC) Layers for MEMS Applications. Physics and Technology of Silicon Carbide Devices, 2012.
24. Silva CM, Katoh Y, Voit SL, Snead LL. Chemical reactivity of CVC and CVD SiC with UO_2 at high temperatures. Journal of Nuclear Materials. 2015; 460:52–59.
25. Balzani V, Venturi M, Credi A. Molecular Devices and machines: A Journey into the Nano World, Wiley-VCH: Weinheim, 2003.
26. Setaka W, Ohmizu S, Kabuto C, Kira M. A Molecular Gyroscope Having Phenylene Rotator Encased in Three-Spoke Silicon-Based Stator. Chemistry Letter. 2007; 36:1076–1077.

27. Setaka W, Ohmizu S, Kira M. Molecular gyroscope having a halogen-substituted *p*-phenylene rotator and silaalkane chain stators. Chemistry Letter. 2010; 39:468–469.
28. Marahatta AB, Kanno M, Hoki K, Setaka W, Irle S, Kono H. Theoretical Investigation of the Structures and Dynamics of Crystalline Molecular Gyroscopes. Journal of Physical Chemistry C. 2012; 116:24845–24854.
29. Marahatta AB, Kono H. Performance of NCC- and SCC-DFTB Methods for Geometries and Energies of Crystalline Molecular Gyroscope. International Journal of Innovative Research and Advanced Studies. 2019; 6(5):180–185.
30. Ehnbom A, Gladysz JA, Gyroscopes and the Chemical Literature, 2002–2020: Approaches to a Nascent Family of Molecular Devices. Chemical Reviews. 2021; 121:3701–3750.
31. Marahatta AB. *Gaussian-External* Methodology Predicted Crystal Structures, Molecular Energetics, and Potential Energy Surface of the Crystalline Molecular Compass. Asian Journal of Applied Chemistry Research. 2023; 14(1): 8–25.
32. Marahatta AB, Kono H. Structural Characterization of Isolated Siloxaalkane Molecular Gyroscopes via DFTB-based Quantum Mechanical Model. International Journal of Innovative Research and Advanced Studies. 2021; 26(1):526–541.
33. Marahatta AB, Kono H. SCC-DFTB Study for the Structural Analysis of Crystalline Molecular Compasses. Chemistry Research Journal. 2022; 7(4):77–94.
34. (a) NIST Chemistry WebBook, SRD 69. Mass Spectrum: 1,4-Bis(trimethylsilyl)benzene Available: https://webbook.nist.gov/cgi/cbook.cgi?ID=C13183705&Units=SI&Mask=200#Mass-Spec

(b) Internal Standard Reference Data for qNMR: 1,4-Bis(trimethylsilyl)benzene, BIPM ISRD-06.

Available: https://www.bipm.org/documents/20126/27085544/bipm%20publication-ID-3286/6fc31b65-bb6c-805d-9f3c-3d318e9d09fc

35. Aradi B, Hourahine B, Frauenheim T. DFTB+, a Sparse Matrix-Based Implementation of the DFTB Method. Journal of Physical Chemistry A. 2007; 111:5678−5684.
36. Elstner M, Frauenheim Th, Kaxiras E, Seifert G, Suhai S. A Self-Consistent Charge Density-Functional Based Tight-Binding Scheme for Large Biomolecules. Physica Status Solidi B. 2000; 217:357−376.
37. Elstner M, Hobza P, Frauenheim Th, Suhai S, Kaxiras E. Hydrogen bonding and stacking interactions of nucleic acid base pairs: A density-functional-theory based treatment. The Journal of Chemical Physics. 2001; 114:5149−5155.
38. Elstner M, Porezag D, Jungnickel G, Elsner J, Haugk M, Frauenheim T, Suhai S, Seifert G. Self-consistent-charge density-functional tight-binding method for simulations of complex materials properties. Physical Review B. 1998; 58:7260−7268.
39. Kohn W, Sham L. Self-Consistent Equations Including Exchange and Correlation Effects. Physical Review Journal. 1965; 140:A1133−A1138.
40. Porezag D, Frauenheim Th, Kohler T, Siefert G, Kaschner R. Construction of tight-binding-like potentials on the basis of density-functional theory: Application to carbon. Physical Review B. 1995; 51:12947−12957.
41. Seifert G. Tight-Binding Density Functional Theory: An Approximate Kohn−Sham DFT Scheme. Journal of Physical Chemistry A, 2007; 111:5609−5613.

42. (a)Macrae CF, Edgington PR, McCabe P, Pidcock E, Shields GP, Taylor R, Towler M, van de Streek J. Mercury: Visualization and Analysis of Crystal Structures. Journal of Applied Crystallography. 2006; 39:453–457.

(b) Jmol: An open-source Java viewer for chemical structures in 3D.

Available: *http://www.jmol.org/*

43. DFTB+ Version 1.3 USER MANUAL.

Available: *https://dftbplus.org/fileadmin/DFTBPLUS/public/ dftbplus/latest/manual. pdf*

44. Benkeser RA, Krysiak HR. The Conjugative Ability of the Trimethylsilyl Group. Journal of American Chemical Society. 1953; 75(10): 2421–2425.